Ab Initio Investigation of Reaction Pathways for Intramolecular Charge Transfer in Dimethylanilino Derivatives

A. L. Sobolewski

Institute of Physics, Polish Academy of Sciences, 02 668 Warsaw, Poland

W. Sudholt and W. Domcke

Institute of Theoretical Chemistry, Heinrich-Heine-University, D-40225 Düsseldorf, Germany

Received: December 5, 1997; In Final Form: February 13, 1998

Minimum-energy paths relevant for intramolecular charge transfer (ICT) in 4-(dimethylamino)benzonitrile (DMABN) and in 4-(dimethylamino)benzethyne (DMABE) have been theoretically investigated. They are expected to characterize the "twisted"-ICT (TICT) and the "rehybridized"-ICT (RICT) photoprocesses. Reaction paths for the L_a and L_b states and the RICT state have been determined at the CIS level. The energy profiles along the reaction paths have been calculated with the CIS, CASSCF, and CASPT2 electronic structure theory methods. It is concluded that stabilization of the L_a state along the TICT reaction path is responsible for appearance of the CT emission in DMABN in polar solvents. The absence of CT fluorescence in DMABE in polar solvents is tentatively attributed to fluorescence quenching by the RICT state.

1. Introduction

4-(Dimethylamino)benzonitrile (DMABN) and its derivatives have been the subject of extensive experimental and theoretical investigations since the discovery of the dual fluorescence of the parent compound in polar solvents.[1] Despite this effort and numerous papers devoted to this subject published over several decades, the mechanism of the intramolecular charge-transfer (ICT) process responsible for the dual emission in polar solvents still is not well understood.

Among the conflicting interpretations,[2−7] the twisted-ICT (TICT) concept (see Scheme 1) introduced by Grabowski et al.,[2,3] is nowadays most widely accepted. The potential-energy (PE) functions of DMABN versus the twist angle of the amino group were computed with semiempirical and ab initio methods and with inclusion of solvent effects.[8−15] These theoretical studies generally provide qualitative support for the original TICT model. They indicate that under isolated molecule conditions the charge-transfer (CT) configuration which may be responsible for dual emission is higher in energy than the "locally excited" (LE) S_1 state. Thus interaction with a polar solvent is necessary for the CT emission to appear. A limitation of the above-mentioned investigations is that they have defined from the outset a reaction coordinate of the process (the twisting of the amino group), while the other intramolecular degrees of freedom are kept frozen (in most cases at experimentally or theoretically determined values for the ground state). Thus the PE functions calculated versus the reaction coordinate cannot generally be expected to follow closely the PE valley that connects the reactant (LE state) to the product (CT state) but rather cut through a slope of the multidimensional PE surface.

An alternative proposal for the ICT reaction coordinate in DMABN and related compounds has been put forward by Zachariasse and collaborators.[6,7] According to this proposal, vibronic coupling between the closely spaced S_1 and S_2 states via the amino inversion mode is primarily responsible for the ICT process in polar solvents. Recent ab initio calculations on isolated DMABN did not provide, however, support for this vibronic-coupling mechanism.[12]

SCHEME 1

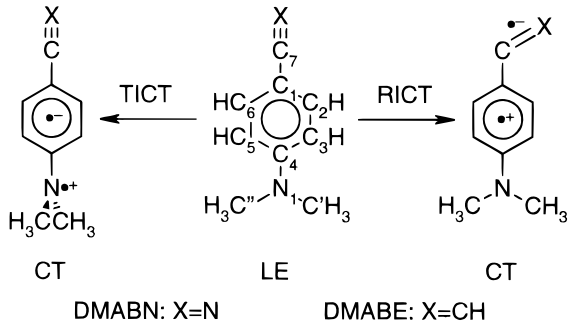

In previous work we have optimized single points on the lowest excited singlet state PE surfaces which are expected to represent structures relevant for the ICT reaction in DMABN and related systems;[16−18] see also ref 19. Besides the polar structure corresponding to a perpendicular conformation of the amino group (the "TICT"-like state), a second local minimum with $sp \rightarrow sp^2$ rehybridized cyano group (the "rehybridized"-ICT, RICT state; see Scheme 1) has been localized on the PE surface of the lowest excited singlet state in the CI singles (CIS) approximation. In the case of DMABN the energies of both structures (TICT and RICT), calculated at the CASPT2 level, were found to be higher in energy than the vertical (Franck−Condon) excitation to the LE state. If, however, the cyano group of DMABN is replaced by the ethyne group, to give 4-(dimethylamino)benzethyne (DMABE), the RICT structure was found to represent the global minimum on the PE surface of the lowest excited singlet state.[17] This result suggests that DMABE may provide an opportunity to study the ICT reaction under isolated molecule conditions. Recent experimental work[20] motivated by this theoretical prediction did not find, however, evidence of a secondary emission band in this compound, neither in nonpolar nor in polar solvents. In view of this negative result,

S1089-5639(98)00435-6 CCC: $15.00
Published on Web 03/28/1998

it has been concluded in ref 20 that no ICT occurs in DMABE in either polar or nonpolar solvents.

In this work we report the results of a more systematic study of reaction paths for the ICT process. In contrast to existing calculations, where a single internal coordinate has been varied, we have constructed the minimum-energy path (MEP) on the PE surfaces of interest. The excited-state geometry optimizations have been performed at the CIS level. PE profiles along the reaction path have subsequently been obtained at higher levels of the theory (CASSCF and CASPT2). Two reaction paths are considered, which connect the vertically excited system (the reactant) with the previously determined TICT and RICT structures (the photoproducts), respectively. In addition to DMABN, we have performed calculations for DMABE in order to shed additional light on the apparent discrepancy between theoretical predictions[18] and experimental observations[20] for this system.

2. Computational Methods

2.1. Geometry Optimizations. The ground-state geometry of DMABN and DMABE has been optimized with the use of the HF and MP2 methods. At both levels of theory the molecular systems are unstable at planar geometry (C_{2v} symmetry). The MP2/6-31G(d) imaginary frequency (131 cm^{-1} for DMABN and 151 cm^{-1} for DMABE) represents the inversion mode of the dimethylamino group. Relaxing the symmetry to C_s stabilizes the systems by 178 and 285 cm^{-1}, respectively, and the angle between the benzene plane and the C−N−C plane of the dimethylamino group is 28.8° for DMABN and 32.2° for DMABE. This calculated (MP2) inversion angle for DMABN is, however, larger than the value of 15° estimated from microwave spectroscopy.[21] The force field and the normal modes of the S_0 state in C_s symmetry also have been determined at the MP2/6-31G(d) level. Here the pyramidalization mode of the dimethylamino group mixes strongly with other kinds of out-of-plane motion; in both systems the lowest frequency mode with inversion character is comparable to the barrier for inversion.

We have adopted the MEP approach to construct the reaction paths for the TICT and RICT processes. According to this method one defines one of the $3N - 6$ internal degrees of freedom as the reaction coordinate, while the remaining internal coordinates are optimized for each value of the reaction coordinate.

The reaction coordinate associated with the TICT process is the torsional angle θ of the dimethylamino group, defined as $\theta = (\tau_1 + \tau_2)/2$, where τ_1, τ_2 are dihedral angles: $\tau_1 = C_3C_4N_1C'$ and $\tau_2 = C_5C_4N_1C''$ (see Scheme 1 for enumeration of the atoms). The torsional angle θ has been varied between 0 and 90° in steps of 15°, and the remaining internal coordinates have been optimized according to the MEP principle for both L_a and L_b states. To avoid variational collapse of the S_2 state to the S_1 state during the optimization, the pyramidalization angle $\delta = (\tau_1 - \tau_2)/2$ was kept frozen at 0°. Therefore C_2 symmetry is retained along the TICT reaction path, and both states can individually be optimized since they belong to different symmetry species, *A* and *B*, respectively. Calculations of the reaction path on the lowest excited singlet state without any symmetry constraints were done for comparison. More detailed investigations of the influence of amino group pyramidalization on the TICT reaction pathway in DMABN will be described in a forthcoming publication.

The intramolecular stabilization of the CT state associated with the RICT process[16−18] involves primarily bending and stretching of the CN(CC) group in DMABN (DMABE). We have chosen the bond length of the CN(CC) group as the reaction coordinate for the RICT process. C_s symmetry is retained in this case. Moreover, the L_a and L_b states even retain C_{2v} symmetry along this coordinate. The CN(CC) bond lengths have been varied from 1.14(1.20) to 1.34(1.45) Å.

TABLE 1: Calculated Harmonic Frequencies (Unscaled) for the S_0, L_a, and RICT States of DMABN and DMABE

state	method[a]	frequency[b]	IR intensity[c]	assignment
		DMABN		
S_0	HF	2592	127	$C{\equiv}N$
	MP2	2204	12	$C{\equiv}N$
L_a	CIS	2378	25	$C{\equiv}N$
RICT	CIS	1259	766	$C-C{\equiv}$
		1515	634	$C-N<$
		1649	21	$C{\equiv}N$
		1770	946	quinoid stretch
		DMABE		
S_0	HF	2402	28	$C{\equiv}C$
	MP2	2157	3	$C{\equiv}C$
L_a	CIS	2023	89	$C{\equiv}C$
RICT	CIS	1258	556	$C-C{\equiv}$
		1511	548	$C-N<$
		1732	64	$C{\equiv}C$
		1775	863	quinoid stretch

[a] 6-31G(d) basis set. [b] In cm^{-1}. [c] In km mol^{-1}.

Optimizations of the excited-state geometries were performed in the CIS approximation.[22] The 6-31G(d) basis set (with polarization functions on heavy atoms) was used in the optimizations and in the calculations of vibrational frequencies at the local minima. These calculations were performed with the GAUSSIAN94 program package.[23]

Unconstrained optimization of the lowest excited singlet state yields a nonplanar structure (C_1 symmetry) with $\tau_1 = 48.9°$, $\tau_2 = 19.1°$ for DMABN, and with $\tau_1 = 51.2°$, $\tau_2 = 15.6°$ for DMABE when starting from the ground-state geometry. In the case of DMABN this corresponds to the structure optimized by Scholes et al.[19] Optimization of the lowest CT state of A'' symmetry in the C_s point group (with the symmetry and the molecular planes coincident) stabilizes the systems in the RICT configuration with bond lengths $C_7N = 1.2785$ Å and $C_7C = 1.3501$ Å, and with bond angles $C_1C_7N = 124.9°$ and $C_1C_7C = 129.3°$ for DMABN and DMABE, respectively. Calculations of the Hessian at the optimized geometry show that all frequencies are real. The RICT state thus represents a local minimum in both systems at this level of theory.

The characteristic feature of the RICT configuration is that it has no typical triple-bond stretching frequency. The frequency of this mode is strongly reduced compared to the S_0 and L_a states due to rehybridization of the cyano (acetyleno) group and is embedded in the dense manifold of the aromatic ring modes in the range 1000−2000 cm^{-1} (see Table 1).

2.2. Energy Calculations. The CASSCF method[24] was used to calculate the energy and one-electron properties of the systems in a given electronic state along the MEP reaction coordinate. The active space was designed by maximizing the weight of the CASSCF reference in the first-order CASPT2 wave function (vide infra). Generally, we have found that an active space comprising 12 electrons for the C_{2v} and C_2 point groups, and 16 electrons for the C_s point group, distributed over 12 molecular orbitals, gives the best description of the electronic wave function at the variational (CASSCF) level. The active space includes the (2−3a_2, 2−9b_1, 12−13b_2), (22−23*a*, 13−22*b*), and (32−33a', 1−10 a'') orbitals in the C_{2v}, C_2, and C_s point groups, respectively.

In the final stage, dynamic electron-correlation effects were added with the use of multiconfiguration second-order perturba-

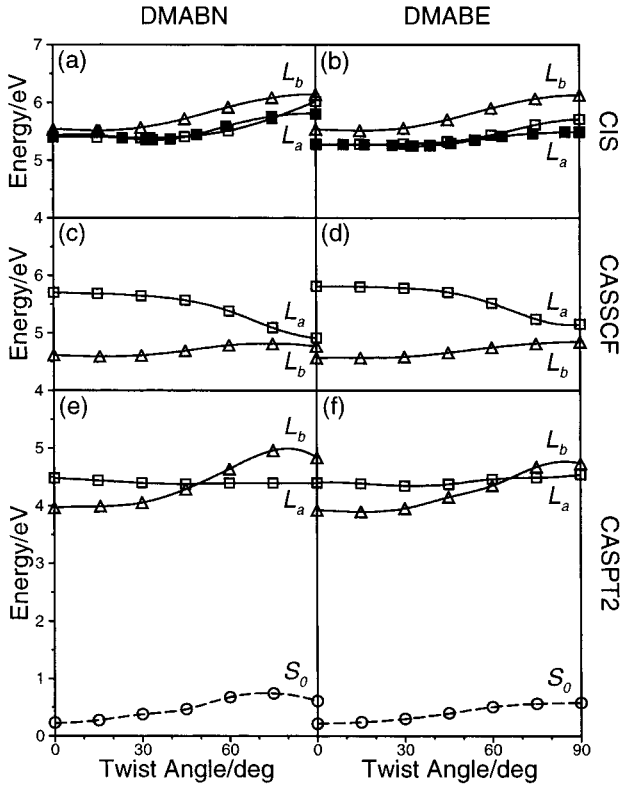

Figure 1. Potential-energy functions of the L_a (squares) and L_b (triangles) states of DMABN (left hand side) and DMABE (right hand side) calculated along the twisting coordinate. (a, b) CIS energy optimized with C_2 symmetry constraint (solid squares denote the S_1 energy optimized without symmetry constraint); (c, d) CASSCF energy, calculated at the CIS(C_2)-optimized geometry; (e, f) CASPT2 energy, including CASPT2 energy of the S_0 state calculated along the L_a reaction path (circles). Energies are given with respect to the energy calculated at the C_{2v} minimum of the ground state with the use of the HF (a, b), CASSCF (c, d), and CASPT2 (e, f) methods.

tion theory, taking the CASSCF wave function as the reference (CASPT2).[25] The value of the (normalized) reference weight gives information on the quality of the perturbational approach. For the active spaces used in these calculations the reference weights were generally in the range 0.6−0.7. This is within the limits of the applicability of the CASPT2 method for systems of such a size, which can be estimated from the approximate formula given in ref 25.

All the CASSCF/CASPT2 calculations were performed with the MOLCAS3 program package.[26] The ANO-L(3s2p1d/2s) basis set was employed, which is of similar quality as the basis set used in the geometry optimizations.

3. Results

3.1. TICT Reaction Path. The energy profiles along the TICT reaction path obtained at the CIS, CASSCF and CASPT2 levels are collected in Figure 1 for DMABN (lhs) and DMABE (rhs). The energy is given in electronvolts relative to the ground-state energy calculated at the corresponding level of theory at the C_{2v}-optimized ground-state geometry (MP2/6-31G-(d) level). These energies are −455.512 96, −455.761 20, −457.037 95, and −439.452 35, −439.679 39, −440.940 40 (in atomic units) at the HF, CASSCF, and CASPT2 levels for DMABN and DMABE, respectively.

Let us first consider the CIS energy profiles in Figure 1a,b. It is seen that the L_b state lies above the L_a state for all twist angles at this level of theory. At the planar geometry this ordering is in contradiction to experiment (cf., for instance, ref 20). In both systems and for both states the PE functions exhibit shallow minima mostly at nonplanar geometry ($\theta \simeq 15°$ for L_b, and $\theta \simeq 30°$ for L_a) and maxima at the perpendicular geometry. The energy profile of the lowest excited singlet state obtained without symmetry restrictions (*i.e.*, allowing pyramidalization of the amino group) follows closely the L_a energy, with the largest difference at perpendicular geometry. This PE function (curve with full squares in Figure 1) also exhibits a shallow minimum near $\theta \simeq 30°$ for both molecules (see discussion in Section 2.1).

Figure 1c,d shows the energy profiles of the L_a and L_b states calculated at the CASSCF level (recall that the geometries of (c,d) are identical with those of (a,b); only the electronic-structure method is different). It is seen that the ordering of the states and the shape of the PE functions differs strongly from the CIS result. The ordering of the CASSCF vertical energies is correct, but the energy gap at $\theta = 0°$ is significantly too large. The shape of the CASSCF PE function of the L_a state is even qualitatively different from the CIS result: the planar geometry corresponds to a maximum, while the perpendicular conformation corresponds to a minimum of the CASSCF PE function.

The energy profiles obtained at the CASPT2 level are shown in Figure 1e,f. CASPT2 energies of the S_0 state evaluated along the L_a-state optimized reaction path are also included. Now the calculated splitting of the L_a and L_b states (the separation of the 0−0 lines for transitions from the ground state), 4100 cm^{-1} for DMABN and 3800 cm^{-1} for DMABE, is in a good accordance with experimental estimates[20] (the 0−0 lines are not, however, directly observed in these systems). It is seen that the effect of dynamical electron correlation again leads to a qualitative change of the PE profile of the L_a state: the L_a energy becomes an extremely flat (on this energy scale) function of the TICT coordinate. This is in contrast to the PE functions of the L_b and the S_0 states, which show significant barriers for rotation of the amino group. The CASPT2 PE function of the L_a state has a very shallow minimum around $\theta \simeq 45°$ for DMABN and around $\theta \simeq 30°$ for DMABE. The planar and perpendicular conformations now represent maxima on the PE curves of the L_a state in both molecular systems. The L_b state, on the other hand, has its minimum close to the planar geometry (within the C_2 symmetry constraint) and a barrier for rotation of the amino group of about 1 eV. The PE curves of both states intersect close to the minimum of the L_a state along the TICT reaction path.

The CASPT2 results of Figure 1e are qualitatively consistent with the PE functions of Serrano-Andrés et al., which were obtained as a function of the twist angle, keeping all other internal coordinates frozen at the ground-state equilibrium value.[12] In particular, the flatness of the L_a state PE function and a minimum at intermediate twist angles ($\theta \simeq 60°$) is in agreement with the present findings. One must keep in mind, however, that in the approach presented here synchronous rotation of the two methyl groups is allowed along the C_2 reaction path, resulting, for example, in an energy lowering of the ground state at 90° in DMABN.

The dipole moments as a function of the reaction path calculated in the CASSCF approximation for the S_0, L_b, and L_a states of DMABN and DMABE are shown in Figure 2a,b, respectively. It is seen that in both systems the dipole moments of the S_0 and L_b states are very similar and are both decreasing functions of the TICT reaction coordinate. The dipole moment of the L_a state is much larger, reflecting its CT character, and

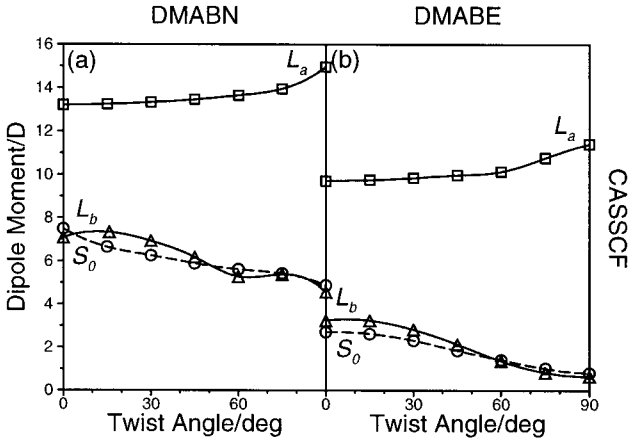

Figure 2. CASSCF dipole moments of the L_a (squares) and L_b (triangles) states of DMABN (a) and DMABE (b) calculated at the CIS(C_2)-optimized geometry of each electronic state along the twisting coordinate. Circles connected by a dashed line denote the dipole moment function of the ground state calculated at the L_a-state optimized geometry.

increases with the reaction coordinate. The dipole moments in DMABE behave similarly, but are altogether smaller than in DMABN. Qualitatively, our findings for DMABN are very similar to those of Serrano-Andrés et al. for rigid twisting of the dimethylamino group.

3.2. RICT Reaction Path. PE functions along the RICT reaction path (stretching of the CN(CC) group) have been computed as described above. The resulting energy curves are shown in Figure 3. In addition to the L_a and L_b states, the energy of the RICT state is indicated in Figure 3. This state transforms according to the A_2 representation in C_{2v} symmetry and the A'' representation in C_s symmetry, respectively. At the S_0 equilibrium geometry and along the TICT reaction path, this state is much higher in energy than the L_a and L_b states and thus irrelevant for the ICT process. The RICT reaction coordinate, however, strongly stabilizes this CT state. In DMABE it becomes the lowest excited singlet state at its optimized geometry.[17]

The PE profiles of the three (L_a, L_b, and A'') states calculated at the CIS level along the RICT reaction path are shown in Figure 3a,b for DMABN and DMABE, respectively. As noted above, the ordering of the L_a and L_b states is incorrect in the CIS approximation. It is seen that the energies of the L_a and L_b states increase along the reaction path, while the energy of the A'' state is significantly lowered. At this level of theory, the A'' state becomes the lowest excited singlet state in both systems already for relatively small stretching of the CN(CC) bond.

The energy profiles obtained at the CASSCF level along the same reaction paths are shown in Figure 3c,d for both systems, respectively. Near-degeneracy effects included in the CASSCF approximation stabilize the L_a and L_b states much more than the A'' state. The ordering of the L_a and L_b states is interchanged with respect to the CIS approximation, but, as noted above, the L_a-L_b energy gap is too large in the CASSCF approximation. The energy of the RICT state relative to the L_a and L_b states is much higher than in the CIS approximation. In remarkable contrast to the TICT reaction path (cf. Figure 1a−d) it is found here that the shape of the PE curves is practically the same in the CIS and CASSCF approximations.

The CASPT2 PE functions are given in Figure 3e,f. The S_0 PE function included in these figures was calculated along the reaction path of the A'' state. It is seen that dynamical electron-

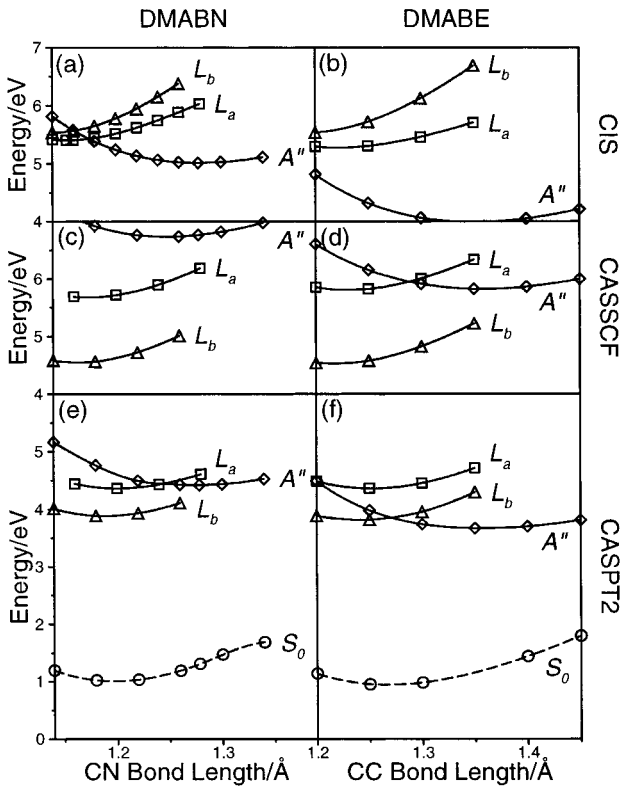

Figure 3. Potential-energy functions of the L_a (squares), L_b (triangles), and RICT (A'') (diamonds) states of DMABN (left hand side) and DMABE (right hand side) calculated along the CN(CC) stretching coordinate. (a, b) CIS energy optimized with C_{2v} (L_a, L_b) and C_s (A'') symmetry constraint; (c, d) CASSCF energy, calculated at the CIS(C_{2v} or C_s)-optimized geometry; (e, f) CASPT2 energy, including CASPT2 energy of the S_0 state calculated along the reaction path of the RICT (A'') state (circles). Energies are given with respect to the energy calculated at the C_{2v} minimum of the ground state with the use of the HF (a, b), CASSCF (c, d), and CASPT2 (e, f) methods.

correlation effects do not significantly affect the shape of the PE profiles, again in contrast to the TICT reaction path. The energy of the RICT state of A'' symmetry is lower in DMABE than in DMABN, as predicted previously.[17] In DMABN, the A'' state is found slightly above the L_a state at the PE minimum of the latter; in DMABE, on the other hand, the A'' state is located below the L_a state at the minimum of the latter. As will be discussed below, this is expected to have significant implications for the fluorescence properties of these systems. It should be stressed, however, that the apparent crossings of the PE functions in Figure 3 are not true crossings, as the three excited-state PE functions in Figure 3 correspond to three different reaction paths, that is, the optimized values of the remaining internal coordinates are different for each state. The CASSCF dipole moments as a function of the RICT reaction coordinate are shown in Figure 4a,b for DMABN and DMABE, respectively. One can easily distinguish between the polar A'' and L_a states, and the nonpolar L_b and S_0 states. The dipole moments in DMABE are systematically smaller than the dipole moments in DMABN as noted before. Although the dipole moment of the A'' states decreases somewhat along the reaction coordinate, it is still significantly higher than those of the nonpolar states.

4. Discussion and Conclusions

4.1. Electronic-Structure Aspects. The results of the present study shed some light on the difficulties that are encountered in the ab initio calculation of photophysical reaction

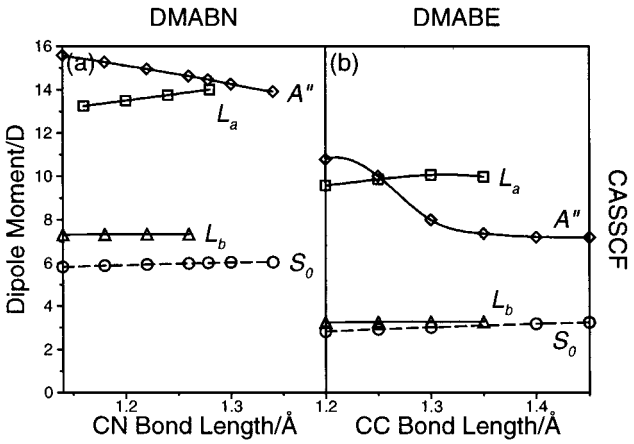

Figure 4. CASSCF dipole moments of the L_a (squares), L_b (triangles), and RICT (A'') (diamonds) states of DMABN (a) and DMABE (b) calculated at the CIS(C_{2v} or C_s)-optimized geometry of each electronic state along the CN(CC) stretching coordinate. Circles connected by a dashed line denote the dipole moment function of the ground state calculated at the RICT(A'')-state optimized geometry.

pathways in polyatomic systems. The results demonstrate, in particular, how dangerous it can be to draw conclusions regarding the mechanism of a photoreaction on the basis of approximate electronic-structure methods. The comparison of the CIS, CASSCF, and CASPT2 results clearly reveals the decisive role of both nondynamical electron correlation effects as well as dynamical correlation effects for excited electronic states. Both the vertical excitation energies and energetic ordering of the states as well as the shape of the PE functions along the reaction paths are generally strongly affected by electron correlation.

The results of Figures 1 and 3 reveal the unreliability of the CIS approximation as far as the energetic ordering of the states and the qualitative shape of PE functions is concerned. Let us briefly discuss the pitfalls that are encountered when calculating excited states of DMABN at the CIS level. At this level of approximation one finds several low-lying excited electronic states, none of which can a priori be excluded from consideration. Neither the energies nor the dipole moments determined at this level of theory are decisive in this respect. Only the confirmation of these results at a more refined level of theory can provide the basis for the selection of the relevant states. A typical example is the L_a state of DMABN. This is the lowest excited singlet state in the CIS approximation (Figure 1a). Moreover, its dipole moment calculated at this level of theory ($\mu = 8.9$ D[19]) is close to the experimental values reported for the ground and the L_b(*LE*) states.[27] As a result of this coincidence, this state has erroneously been identified as the locally excited L_b state in ref 19. Within the C_1 point group the L_a and L_b states cannot be distinguished by symmetry, but they can be correlated adiabatically to the respective L_a(*A*) and L_b(*B*) states calculated within the C_2 symmetry constraint. Decisive for the identification of these states is the oscillator strength for transitions from/to the ground state ($f \simeq 0.35$ for L_a and $f \simeq 0.02$ for L_b, calculated at the ground-state optimized geometry with the CASSCF method[17]). The CIS value of $f \simeq 0.5$ obtained at the optimized geometry of the "lowest" excited singlet state[19] clearly indicates that this state correlates adiabatically to the $L_a(A_1)$ state at planar geometry. The small value of the dipole moment of this state is an artifact of the CIS approximation. At the perpendicular conformation of the amino group, if one imposes C_{2v} symmetry, the L_a state has A_2 symmetry and is thus forbidden in absorption from the ground state. It possesses, contrary to the CIS result of ref 19, a large dipole moment (Figure 2a). At this geometry there are actually two close-lying excited singlet states in the CIS approximation, the second of which belongs to the A_1 representation and has the oscillator strength $f \simeq 0.4$ at the CIS level. The lowest CASPT2 energy of an A_1 state is, however, by more than 1.5 eV higher than that of the $L_a(A_2)$ state at $\theta = 90°$. These facts clearly demonstrate that it is impossible, on the basis of CIS energy calculations alone, to develop a reliable picture of the electronic states that are relevant for the spectroscopy and the photochemical dynamics.

Energy calculations at the CASSCF level with a compact active space (the choice of a restricted active space is a necessity for molecules of the size considered here) are likewise insufficient for the construction of reliable photochemical PE functions. As shown in Figures 1 and 3, dynamical electron correlation has a large effect on vertical excitation energies. In the case of the TICT reaction path, the PE function of the L_a state changes even its qualitative shape upon inclusion of electron correlation effects.

At present the CASPT2 method is the only ab initio method that includes both near-degeneracy as well as dynamical correlation effects and is feasible for molecules of this size. One should have in mind, of course, the limitations of the perturbational method. This particularly concerns situations where only a relatively small amount of electron correlation effects is included at the variational (CASSCF) level. The quality of the CASPT2 result is generally reflected by the weight of the CASSCF reference in the first-order wave function. For the active spaces used in this work (12−16 electrons correlated in 12 orbitals) this value is well within the limits that one can estimate on the basis of the formula given in ref 25 as being appropriate for systems of such size. The weight of the CASSCF reference is characteristic for a given electronic state but also shows some variation along the reaction path.

It may be interesting to note that there is a significant difference in the CASPT2 calculations for the RICT and the TICT reaction paths. In the former case the molecule remains planar along the reaction path. Thus there is a natural recipe for the choice of the active space: include as many π-orbitals as possible, which are relevant for the lowest electronic states of $\pi\pi^*$ character, and add some σ-orbitals relevant for the RICT state. Because the $\sigma-\pi$ separation is conserved along the reaction path, convergence in the CASSCF cycle is efficient and does not strongly depend on the starting orbitals. This is not the case for the TICT reaction path. Here the molecule is nonplanar, and there is a significant mixing of the "important" orbitals of π origin with relatively "unimportant" orbitals of σ origin that belong to the same symmetry block. It often happens that at a given geometry the CASSCF iteration converges to different close-lying "local" minima of the energy functional, depending on the initial guess for the orbitals. In most cases this can be recognized by comparing the CASSCF energy of neighboring points as well as by checking the reference weight in the CASPT2 first-order wave function. Benchmark calculations, at least at the most crucial points of the PE surfaces, with the use of MR-CI methods would be very helpful to confirm the reliability of the CASPT2 results.

4.2. Photophysical Aspects. *4.2.1. DMABN.* The present results for DMABN generally support the TICT hypothesis for the ICT process. The torsion of the dimethylamino group leads to a stabilization of the L_a state which possesses pronounced CT character. In contrast to the original TICT hypothesis,[3] however, twisting to the perpendicular conformation is not

necessary for charge separation to occur. The charges are already significantly separated at the planar geometry of the L_a state, but rotation of the amino group increases further the dipole moment of this state (Figure 2). Moreover, the potential minimum of the L_a state along the TICT reaction coordinate is found at $\theta \simeq 45°$, rather than at $\theta = 90°$. Our calculations show beyond any doubt that the polar CT state in DMABN must be the S_2 (L_a) state. Along the TICT reaction path there is no other CT state close enough in energy which could be involved in the ICT process. This conclusion of the present work is in agreement with ref 12, where CASPT2 energies have been calculated as a function of rigid torsion.

In the isolated molecule, the L_a state is located above the L_b state at the vertical geometry and the two PE functions intersect upon twisting, cf. Figure 1e. This result is consistent with the absence of ICT in the isolated molecule and in nonpolar solvents. In polar solvents, the L_a state is stabilized relative to the L_b (and S_0) state as a consequence of its much higher dipole moment (cf. Figure 2a). This lowers the crossing point and eventually leads to barrierless ICT. The increase of the dipole moment of the L_a state with the twisting angle may result in a shift of the L_a PE minimum to higher twist angles in polar solvents. The fluorescing state is the L_a state (or the L_a-state component in the vibronically mixed S_1-S_2 states) at its minimum geometry. Apart from the modifications mentioned above, the TICT model of ICT and dual fluorescence is supported by the present calculations. For quantitative conclusions, it is necessary to include solvation effects in the ab initio calculations.

As far as the RICT mechanism is concerned, the present results indicate that this ICT process is not expected to compete with the TICT mechanism in DMABN. The RICT state of A'' symmetry is located above the L_a state at the minimum of the latter in the isolated molecule (cf. Figure 3a). The L_a-A'' crossing occurs at a bond length which is ≃0.05 Å larger than the equilibrium bond length of the L_a state. Interaction with a polar solvent stabilizes the A'' state more than the L_a state, moving the crossing closer to the L_a minimum. It seems that the RICT state in DMABN is just high enough in energy in order not to interfere with the fluorescence from the L_a state.

A possibility of identification of the fluorescent state is transient IR spectroscopy as reported in ref 28. In this work the CN stretching frequency of the fluorescing state has been measured to be 2096 cm^{-1}, 120 cm^{-1} lower than in the ground state of DMABN. As described in section 2, we have calculated excited-state vibrational frequencies at the CIS level. The data (vibrational frequencies (unscaled) and IR intensities) for selected modes are given in Table 1. The result for the CN stretching frequency of the twisted L_a state is 2378 cm^{-1}, 214 cm^{-1} lower than the CN stretching frequency estimated for the ground state at the HF level. With all reservations concerning the reliability of CIS (and HF) vibrational frequencies, this agreement provides support that the fluorescing state in DMABN is indeed the twisted L_a state, which exhibits a moderately lowered CN stretching frequency.

4.2.2. DMABE. Overall, the results for the TICT reaction path of DMABE are quite similar to those found for DMABN. We find weak stabilization of the L_a state by twisting (cf. Figure 1f). The stabilization energy is smaller than in DMABN, and the minimum of the PE function is found at a smaller twist angle ($\theta \simeq 30°$). Also the PE barrier at $\theta = 90°$ is higher in DMABE than in DMABN. But as far as the TICT reaction path in the isolated molecule is concerned, we observe no significant differences between DMABE and DMABN.

The dipole moment of the L_a state is significantly smaller in DMABE (cf. Figure 2) and the L_a state of DMABE is thus less stabilized in polar solvents relative to the L_b state. Whether this difference in polarity of the L_a state is responsible for the absence of dual fluorescence of DMABE in acetonitrile[20] cannot be decided at present. A decision of this question has to await accurate calculations of solvatochromic shifts with ab initio methods.

With respect to the RICT reaction path there exists, on the other hand, a significant difference between DMABE and DMABN (cf. Figure 3e,f). Even in the isolated molecule, the RICT state of A'' symmetry is located below the L_a state at the minimum geometry of the latter. We therefore have to expect fast intramolecular nonradiative relaxation from L_a to the A'' state, which is very weakly fluorescent ($f = 0.004$[17]). Moreover, the energy gap between the A'' minimum and the S_0 PE curve is comparatively small, which is indicative of fairly rapid internal conversion to the ground state. We may thus tentatively explain the absence of dual fluorescence in DMABE in polar solvents via the quenching of the ICT fluorescence by the RICT state.

Transient IR spectroscopy might provide a possibility to detect the RICT state as a short-lived intermediate in the ICT dynamics of DMABE in polar solvents. A characteristic feature of the RICT state is the lack of a triple-bond CC frequency. The CIS calculation predicts a CC stretching frequency of 1732 cm^{-1} for the RICT state, which is very much lower than the acetylenic CC stretching frequency in the electronic ground state (2402 and 2157 cm^{-1} at the HF and MP2 levels, respectively; see Table 1). While the intensity of the CC stretching line in the RICT state is only moderate (and is embedded into a dense manifold of aromatic ring modes), the CIS calculation predicts a characteristic pattern of three very intense lines in the 1000−2000 cm^{-1} range typical for stretching modes of aromatic systems (see Table 1). These three intense IR bands may serve as a fingerprint of the RICT state and may possibly allow the identification of its role in the photophysics of DMABE.

Acknowledgment. This work has been supported by the Fonds der Chemischen Industrie, the Deutsche Forschungsgemeinschaft, and the Committee for Scientific Research of Poland (Grant 2 PO3B 035 13).

References and Notes

(1) Lippert, E.; Lüder, W.; Moll, F.; Nägele, W.; Boos, H.; Prigge, H.; Seibold-Blankenstein, I. *Angew. Chem.* **1961**, *73*, 695.
(2) Rotkiewicz, K.; Grellmann, K. H.; Grabowski, Z. R. *Chem. Phys. Lett.* **1973**, *19*, 315.
(3) Grabowski, Z. R.; Rotkiewicz, K.; Siemiarczuk, A.; Cowley, D. J.; Baumann, W. *Nouv. J. Chim.* **1979**, *3*, 443.
(4) Lippert, E.; Rettig, W.; Bonačić-Koutecký, V.; Heisel, F.; Miehé, J. A. *Adv. Chem. Phys.* **1987**, *68*, 1.
(5) Weisenborn, P. C.; Huizer, A. H.; Varma, C. A. G. O. *Chem. Phys.* **1989**, *133*, 437.
(6) Zachariasse, K. A.; von der Haar, Th.; Hebecker, A.; Leinhos, U.; Kühnle, W. *Pure Appl. Chem.* **1993**, *65*, 1745.
(7) van der Haar, Th.; Hebecker, A.; Il'ichev, Y.; Jing, Y.-B.; Kühnle, W.; Zachariasse, K. *Recl. Trav. Chim. Pays-Bas* **1995**, *114*, 430.
(8) LaFemina, J. P.; Duke, C. B.; Paton, A. *J. Chem. Phys.* **1987**, *87*, 2151.
(9) Majumdar, D.; Sen, R.; Bhattacharyya, K.; Bhattacharyya, S. P. *J. Phys. Chem.* **1991**, *95*, 4324.
(10) Broo, A.; Zerner, M. C. *Theor. Chim. Acta* **1995**, *90*, 383.
(11) Hayashi, S.; Ando, K.; Kato, S. *J. Phys. Chem.* **1995**, *99*, 955.
(12) Serrano-Andrés, L.; Merchán, M.; Roos, B. O.; Lindh, R. *J. Am. Chem. Soc.* **1995**, *117*, 3189.
(13) Nordio, P. L.; Polimeno, A.; Saielli, G. *J. Photochem. Photobiol.* **1997**, *A105*, 269.
(14) Kim, H. J.; Hynes, J. T. *J. Photochem. Photobiol.* **1997**, *A105*, 337.
(15) Gedeck, P.; Schneider, S. *J. Photochem. Photobiol.* **1997**, *A105*, 165.

(16) Sobolewski, A. L.; Domcke, W. *Chem. Phys. Lett.* **1996**, *250*, 428.
(17) Sobolewski, A. L.; Domcke, W. *Chem. Phys. Lett.* **1996**, *259*, 119.
(18) Sobolewski, A. L.; Domcke, W. *J. Photochem. Photobiol.* **1997**, *A105*, 325.
(19) Scholes, G. D.; Phillips, D.; Gould, I. R. *Chem. Phys. Lett.* **1997**, *266*, 521.
(20) Zachariasse, K. A.; Grobys, M.; Tauer, E. *Chem. Phys. Lett.* **1997**, *274*, 372.
(21) Kajimoto, O.; Yokoyama, H.; Ooshima, Y.; Endo, Y. *Chem. Phys. Lett.* **1991**, *179*, 455.
(22) Foresman, J. B.; Head-Gordon, M.; Pople, J. A.; Frisch, M. J. *J. Phys. Chem.* **1992**, *96*, 135.
(23) Frisch, M. J.; Trucks, G. W.; Schlegel, H. B.; Gill, P. M. W.; Johnson, B. G.; Robb, M. A.; Cheeseman, J. R.; Keith, T. A.; Petersson, G. A.; Montgomery, J. A.; Raghavachari, K.; Al-Laham, M. A.; Zakrzewski, V. G.; Ortiz, J. V.; Foresman, J. B.; Cioslowski, J.; Stefanow, B. B.; Nanayakkara, A.; Challacombe, M.; Peng, C. Y.; Ayala, P. Y.; Chen, W.; Wong, M. W.; Andres, J. L.; Replogle, E. S.; Gomperts, R.; Martin, R. L.; Fox, D. J.; Binkley, J. S.; Defrees, D. J.; Baker, J.; Stewart, J. P.; Head-Gordon, M.; Gonzalez, C.; Pople, J. A.; GAUSSIAN 94, Revisions B.3 and D.4; Gaussian Inc.: Pittsburgh, PA, 1995.
(24) Roos, B. O. *Adv. Quantum Chem.* **1987**, *69*, 399.
(25) Andersson, K.; Roos, B. O. In *Modern Electronic Structure Theory*; Yarkony, D. R., Ed.; World Scientific: New York, 1995; p 55.
(26) Andersson, K.; Blomberg, M. R. A.; Fülscher, M. P.; Karlström, G.; Kellö, V.; Lindh, R.; Malmqvist, P.-Å.; Noga, J.; Olsen, J.; Roos, B. O.; Sadlej, A. J.; Siegbahn, P. E. M.; Urban, M.; Widmark, P.-O.; MOLCAS Version 3; University of Lund, Sweden, 1994.
(27) Schuddeboom, W.; Jonker, S. A.; Warman, J. M.; Leinhos, U.; Kühnle, W.; Zachariasse, K. A. *J. Phys. Chem.* **1992**, *96*, 10809.
(28) Hashimoto, M.; Hamaguchi, H. *J. Phys. Chem.* **1995**, *99*, 7875.